ACS Photonics

Article

pubs.acs.org/journal/apchd5

Optical Absorption Imaging by Photothermal Expansion with 4 nm Resolution

Raul D. Rodriguez,*[,†,‡,§] Teresa I. Madeira,[‡] Evgeniya Sheremet,[†,∥] Eugene Bortchagovsky,[⊥] Ashutosh Mukherjee,[‡] Michael Hietschold,[∥] and Dietrich R. T. Zahn[‡,§]

[†]Tomsk Polytechnic University, 30 Lenin Avenue, 634050 Tomsk, Russia

[‡]Semiconductor Physics, Chemnitz University of Technology, D-09107 Chemnitz, Germany

[§]Center for Advancing Electronics Dresden (cfaed), Chemnitz University of Technology, D-09107 Chemnitz, Germany

[∥]Solid Surfaces Analysis Group, Chemnitz University of Technology, D-09107 Chemnitz, Germany

[⊥]Institute of Semiconductor Physics of NASU, Prospekt Nauki 41, Kiev 03028, Ukraine

Supporting Information

ABSTRACT: For quite a long time, one thought of the diffraction limit of light as a fundamental unbreakable barrier that prevents seeing objects with sizes smaller than half the wavelength of light. Super-resolution optical methods and near-field optics enabled overcoming this limitation. Here we report an alternative approach based on tracking the photothermal expansion that a nano-object experiences upon visible light absorption, applied successfully in the characterization of samples with a spatial/lateral resolution down to 4 nm. Our device consists of an atomic force microscope coupled with a solid-state laser and a mechanical chopper synchronized with the natural oscillation mode of an in-house-made gold tip cantilever system. This configuration enhances the detection of nanostructures due to the intermittent light excitation and the consequent intermittent thermal expansion of the sample under investigation. The sensitivity and spatial resolution are further improved by the electric field enhancement due to the excitation of localized surface plasmons at the tip apex. Our concept is demonstrated by the analysis of a two-dimensional material (GaSe) on crystalline sp^2 carbon (graphite) and by an array of multiwalled carbon nanotubes lithographically designed in a SiO_2 matrix. The photothermal expansion originating from light absorption leads to an unprecedented spatial resolution for an optical absorption event imaged below 10 nm.

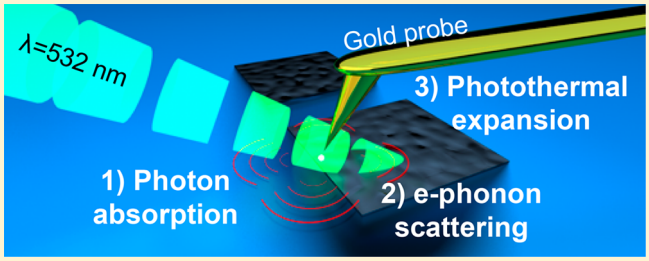

KEYWORDS: *nano-optics, atomic force microscopy, optical absorption, gallium selenide, carbon nanotubes, photothermal-induced resonance, photonics, thermal near field, nanoscale*

In addition to the boom of super-resolution microscopy,[1] the combination of optics and scanning probe microscopy gave way to near-field methods that allow breaking the diffraction limit of light.[2−12] However, the standard microscopy near-field methods were concentrated in the first years to develop imaging with the highest spatial resolution.[13,14] Realizing that, contrary to standard microscopy, the image in near-field optics is produced by scattering, other tasks or other specific systems have been addressed during last years.[4] Despite a variety of near-field optical approaches, the detection of local optical absorption is a challenging task. A considerable contribution to this field has been made by several groups, in particular by Centrone's[15] and Dazzi's.[16] Katzenmeyer et al. recently showed that optical absorption in photothermal-induced resonance (PTIR) could also be obtained in the visible range.[11] However, their findings, as well as most PTIR results reported so far, were achieved using the evanescent field experienced by the sample and originating from a prism illuminated in a total internal reflection geometry.[15,17] Such a configuration is an efficient way to illuminate the sample but has the drawback of being limited to samples that are either very thin or transparent. Development of PTIR allows applying it to the investigation of molecular and lattice vibrations[17,18] and to make it competitive to a few nano-optical methods combining atomic force microscopy (AFM) and spectroscopy such as tip-enhanced Raman spectroscopy (TERS)[6,10] or nanoinfrared.[16] These approaches have been proven to be quite successful in providing information on molecular or lattice vibrations and even plasmon−phonon coupling.[19] A comprehensive survey of the development and the present status of PTIR can be found in the recent review by A. Dazzy.[20] This is particularly the case in AFM-IR and PTIR, which use excitations in the infrared (IR) spectral range. It is then possible to obtain the same information as in a conventional IR spectrometer but with an impressive nanoscale resolution.[21] It is also noticeable that the IR-tunable pulsed lasers used in PTIR can cost as much as the AFM setup itself, making the generalization of this method

Received: May 5, 2018
Published: May 25, 2018

DOI: 10.1021/acsphotonics.8b00590
ACS Photonics XXXX, XXX, XXX−XXX

even more difficult. In this work, we implement a new concept for photothermal expansion in the visible range that overcomes all the limitations mentioned above. Contrary to most previous reports based on the tracking of photothermal expansion due to excitation of molecular vibrations,[18] we aim at investigating the photothermal expansion due to optical absorption in the visible range and its nanoscale mapping with AFM. We refer to this method as *nano-vis*, with its physical mechanism of operation depicted in Figure 1a. Upon resonant photon absorption and

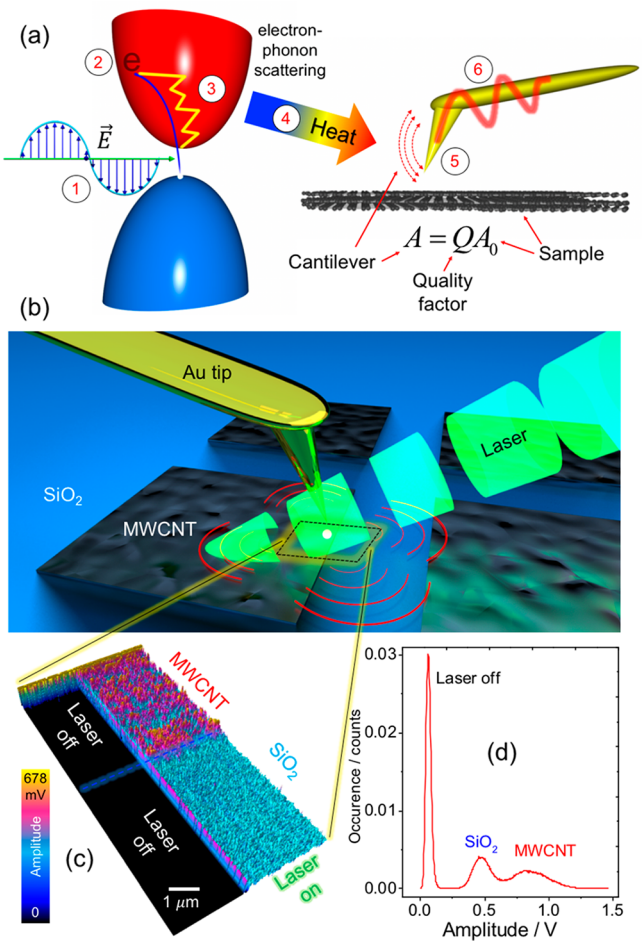

Figure 1. (a) Physical schematics behind nano-vis: (1) a photon with energy well above the energy band gap excites an electron from the valence band to a higher energy level (2) in the conduction band, nonradiative relaxation (3) mediated by e-phonon scattering induces (4) heat generation that results in the thermal expansion of the sample (5) and the cantilever deflection (6). (b) Schematics of the nano-vis experiment with an Au cantilever tip and an MWCNT sample illuminated by a chopped laser beam. (c) Photothermal amplitude image of the MWCNT/SiO_2 interface with half of the image acquired in the dark, laser off. (d) Histogram of the photothermal expansion image shown in (c).

excitation of electrons to higher energy levels in a molecule or crystal, the nonradiative relaxation of charge carriers induces local heating due to electron−phonon scattering. This heating produces the thermal expansion of the nano-object under investigation. The local change of sample size is detected and mapped using an atomic force microscope, allowing in this way the indirect visualization of light absorption. It is necessary to keep in mind that different processes occuring on different time scales, with respect to the modulation frequency, should weight their contribution to the result, and the whole chain of the transformation of the absorbed light into the AFM signal described schematically also includes the thermal conductivity and the elasticity of the object under investigation. Moreover, the registered value proportional to the absorption is also defined by the quantum efficiency of the heat generation, expansion coefficient, and local amount of the absorbing material and depends on the thermal and elastic interactions with the local environment. The signal is produced by a complex mixture of physical parameters from the sample. It is necessary to note in the interpretation that the proposed method is not a straightforward detection of the absorption coefficient, but perhaps it is the only present approach to characterize the absorption at the nanoscale. Similarly to PTIR, the spatial resolution of nano-vis should be limited by the dimensions of the tip apex used in AFM and local field distribution and enhancement around the tip−surface contact. In Table S1 we summarize the main differences between nano-vis and PTIR. Our concept is based on the use of continuous wave (cw) lasers that can be as inexpensive as conventional laser pointers. From one side, the system with several lasers restricts the spectroscopic possibilities of the method, but usually features in the visible spectra are not so narrow as in IR; thus a high spectral resolution may not be necessary. Additionally, having no limitation on the quality of the light excitation like in Raman spectroscopy, further development with the use of a monochromator for the illumination at different wavelengths is probably possible. An intermittent illumination procedure was established to increase the sensitivity of the system to the small sample deformation caused by thermal expansion. Our strategy is based on using a conventional chopper at a frequency matching the mechanical resonance of the AFM cantilever. This results in the resonant enhancement of the cantilever oscillation amplitude induced by the mechanical excitation from the sample. We used a fully metallic Au cantilever with eigenfrequencies below 10 kHz. These metallic probes add the advantage of acting as a highly confined light source due to the excitation of localized surface plasmons at the tip apex. The plasmonic contribution to nano-vis helps to improve the spatial resolution and sensitivity, as shown recently by Belkin's group.[18] We aim at the widespread implementation of nano-vis using off-the-shelf components—a cantilever, chopper, and cw laser—for nanoscale visible absorption imaging with a record spatial resolution below 10 nm.

RESULTS AND DISCUSSION

Proof-of-Concept: Imaging a Carbon Nanotube/Glass Interface. Two different sample kinds were investigated. The first one was a two-dimensional layered material (GaSe) deposited by mechanical exfoliation on a freshly cleaved graphite substrate (HOPG).[22] The second sample consists of vertically aligned multiwalled carbon nanotubes (MWCNTs) embedded in a SiO_2 matrix lithographically defined.[23] In this latest sample, two different MWCNTs were investigated: square-shaped MWCNTs that show a sharp SiO_2/MWCNT interface and MWCNT circular vias. Fully metallic Au cantilevers[24] were used in the AFM experiments operated in contact mode. The cantilever dynamic response[25] was experimentally determined using an AC piezoelectric excitation and tracking of the cantilever oscillation amplitude in the range from 1 to 10 kHz.

DOI: 10.1021/acsphotonics.8b00590
ACS Photonics XXXX, XXX, XXX−XXX

For the nano-vis experiments, the AC piezoelectric excitation was switched off, and the laser chopper frequency was set to the resonance of the cantilever found in that frequency range. The AFM was operated in contact mode during nano-vis. Contrary to previous realizations of PTIR in the visible range[17] we use external illumination and inexpensive off-the-shelf optical components that make a simplified optical scheme. Moreover, we consider the external illumination as the principal difference between the two approaches. On one side, the direct tip illumination makes its own thermal expansion, but the illumination in total internal reflection geometry does not exclude this effect if the prism coverage is not completely opaque. Furtheremore, the scheme with internal reflection is the standard for the so-called photon tunneling (PSTM). PSTM is a variation of scanning near-field optical microscopy (SNOM) where the local field excites the tip and the scattered signal is defined by the sample's topography.[26] This local field would be enhanced and rescattered by the tip interacting with the surface; thus this process could increase the topographic artifacts in PTIR with internal illumination of the object. An additional problem of the internal illumination is the difference of the absorption point situated at the prism−specimen boundary and the tip situated on the other side of the prism coverage. In such a case the registered signal will be affected by local stiffness and elasticity of the specimen and distorted if not seriously corrupted. The nano-vis imaging results of the MWCNT structure shown in Figure 1c confirm the working principle of our method. It is worth noticing that the mechanical and chemical polishing of the sample minimizes the topography differences at the interface. This a crucial point to separate the optical absorption effects from topographic artifacts that could influence the nano-vis contrast. Figure 1c also shows that the contrast completely disappears when the laser excitation is turned off. The amplitude distribution (how often a given amplitude value appears in the image) in Figure 1d clearly shows the different contributions to the nano-vis contrast, as well as its decrease when the laser was turned off. Similar results showing no contrast were obtained for direct illumination not modulated by the chopper and for chopper frequencies much higher or lower than the resonance frequency of the cantilever; see Figure S3 in the Supporting Information. These results confirm the origin of the cantilever amplitude contrast as being due to the photothermal expansion after optical absorption takes place.

Mechanical Resonance Matching: The Key to Achieving High Sensitivity. The typical AFM deflection sensitivity is in the range of 0.1 nm, depending on the optical lever system used for detection. Nano-vis can be sensitive to the thermal expansion of the sample well below that threshold. This high sensitivity is due to the amplification of the cantilever oscillation amplitude (A) at resonance. This amplification occurs when the sample expands and contracts at a frequency matching a mechanical eigenfrequency of the cantilever, making it oscillate at Q (the cantilever quality factor) times the amplitude of the sample ($A = QA_0$). It is this resonance condition that makes possible achieving the high picometer sensitivity down to the expansion of a single molecular layer in the near-IR regime reported previously.[18] In Figure S3 of the Supporting Information, nano-vis images with the chopper in- and off-resonance illustrate this point. If the frequency of the chopper is detuned from the cantilever resonance (Figures S3 and S8) or the sample is illuminated without a chopper or without the laser (Figures S4 and S8), then a decrease in the nano-vis contrast is observed. These results provide additional confirmation of the physical photothermal origin and mechanical resonance dependent sensitivity of the system. A similar approach was recently used. Greco et al. reported on the exploitation of mechanical resonances in a cantilever to study the plasmonic amplification of a single hotspot with modulated Raman spectroscopy.[27]

Spatial Resolution below 10 nm. The spatial resolution of this system is obtained from the cross-sectional analysis in Figure 2. The topography and amplitude images are shown in Figure 2a,b. The cross-section analysis of the amplitude image in Figure 2c shows a remarkable spatial resolution below 10 nm, only limited by the pixel size. Figure 2b even shows some features on the MWCNT not visible in the topography image. These features might be hidden by the tip imaging effects in the topography that are overcome by nano-vis. Notice that when investigating other kinds of samples, the high spatial resolution of ∼4 nm we obtain might vary in other nanoscale systems having larger sample topography features than the sample shown in Figure 2.

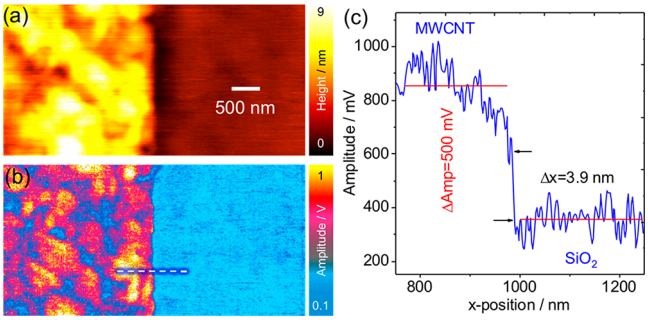

Figure 2. (a) AFM topography image of the MWCNT/SiO_2 interface. (b) Photothermal expansion image (amplitude) showing that the spatial resolution is below 10 nm, limited by the pixel size as shown in the cross-section profile in (c).

The complementarity between the topography and the nano-vis images can be further visualized from the statistical distribution of topography and amplitude values in Figure S5. This analysis shows the noncorrelation between the topography and nano-vis results. If there was a full correlation between the two data sets, then their distributions would also be similar. But as shown in Figure S5, the nano-vis statistical distribution of the contrast can be deconvolved by three Gaussian peaks. The peaks were numerically fit without constraints, reaching an accuracy of 99.9% to the experimental data. Contrary to the contrast for the nano-vis image, the height distribution has several contributions that span a broad range. This is representative of the different topographical features of the MWCNT region.

Nano-vis in 2D Materials: Visualizing Subnanometer Defects in Graphite. Now we turn our focus to the second sample reported in this study: one van der Waals material on top of another one, GaSe on HOPG, shown in the topography AFM image in Figure 3a. The deflection (error) image in Figure 3b shows the homogeneity of the scanning except at the interface due to changes in topography. The photothermal image in Figure 3c, on the other hand, shows a clear contrast between the HOPG and GaSe surfaces. Similarly to the case of the MWCNT, a part of the image was acquired by turning the laser off (top side in Figure 3c). In the photothermal image in Figure 3c, we also observe a stripe-like region giving higher

DOI: 10.1021/acsphotonics.8b00590
ACS Photonics XXXX, XXX, XXX−XXX

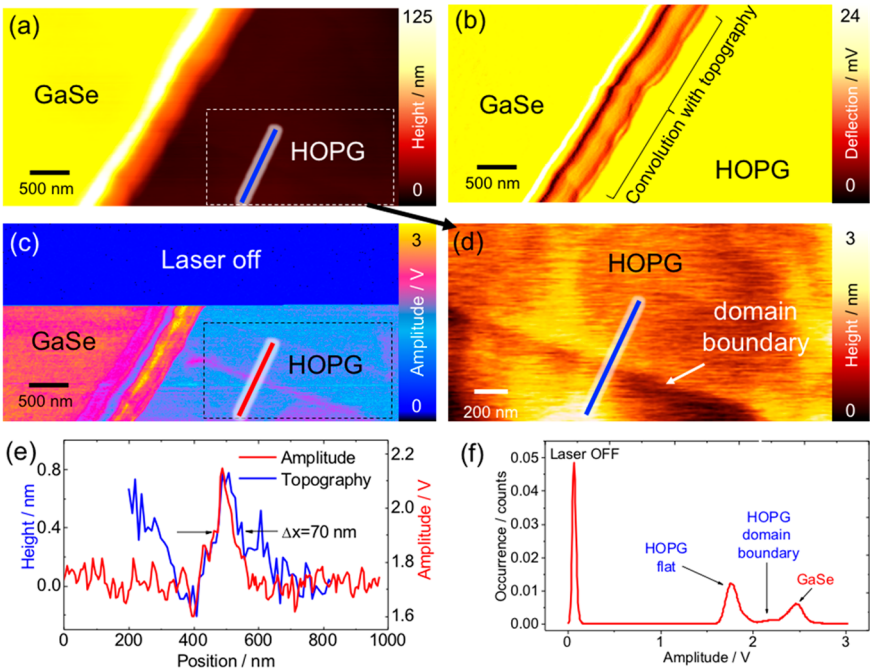

Figure 3. (a) Topography and (b) cantilever deflection image of GaSe on HOPG. (c) Photothermal expansion image with the laser off (top) and laser on (bottom) at the GaSe/HOPG boundary. (d) Zoom-in in the topography of the region marked in (a) and (c) showing a domain boundary in HOPG. (e) Cross-section profiles of the HOPG domain boundary in the regions marked in the photothermal and topography images (a) and (c). (f) Histogram of the photothermal expansion image showing the amplitude distribution for the different tip−sample configurations, including the contribution from the domain boundary.

contrast than the rest of the HOPG surface. This feature on HOPG is not readily visible in the topography or deflection, Figure 3a and b, respectively. For clarity, this region was zoomed-in around the area indicated by the dashed rectangle in Figure 3a and c. The zoom-in of the topography image is shown in Figure 3d. The photothermal and topography cross-sections in Figure 3d are indicated in the images by red and blue lines in Figure 3b and c, respectively. The cross-section profiles across the stripe region on HOPG in Figure 3d show that it consists of a domain boundary of 0.8 nm height. The lateral size of the stripe of about 70 nm can be determined from cross sections made on both the topography and the nano-vis images. Boundaries and folds in graphite can be expected to have higher absorption than its pristine counterpart since such defects add new states for electronic transitions as well as increasing the scattering probability of photoexcited charge carriers. However, one more contribution to the contrast in nano-vis is related to the heat dissipation of the sample. This is discussed below in more detail. Thus, the higher nano-vis contrast for the domain boundary in HOPG may also be related to the defects introduced by the domain boundary that minimize the heat conductivity. This result implies that the nano-vis image has at least the same spatial resolution as the topography obtained by AFM. This observation validates our hypothesis that the lateral spatial resolution in optical absorption and photothermal expansion of nano-vis are limited by the tip size. The effect from the domain boundary is also visible in the amplitude distribution shown in Figure 3f by a small bump below the GaSe peak. This result implies that our method is even sensitive to nanoscopic features with slight differences in optical absorption or heat conductivity. Further application of this method to nanoscaled carbon with sp^2 hybridization (single-walled carbon nanotubes and graphene) could provide new significant insights into the physical and optical properties of these nanomaterials as well as other two-dimensional semiconductors such as MoS_2 and membrane-like metamaterials.[28]

Another observation from the results shown in the deflection image of Figure 3b is the similar contrast between the GaSe and HOPG regions of the sample. The only contrast in cantilever deflection appears at the GaSe/HOPG interface due to the signal convolution with topographical changes of the sample. This result helps us to rule out topographic effects on the nano-vis contrast. It is understandable that the topographical effects are not dominant since both sides of the sample have a roughness (RMS) below 0.5 nm. Similarly, since the domain boundary topography does not even reach 1 nm in height, we can confidently rule out the topography contribution to the nano-vis image of the graphite domain boundary shown in the cross-section (Figure 3e). Topographical and nano-vis (photothermal expansion) data show a correlation between regions that considerably well absorb light (GaSe and MWCNT) and regions with lower absorption or reflective areas (SiO_2 and HOPG, respectively). We verified that exciting the sample by a laser modulated with a chopper set around the mechanical resonance frequency of the cantilever resulted in well-resolved image contrast. Moreover, we observed the decrease in contrast either when the sample was constantly illuminated (non-modulated laser) or when the laser was turned off. In this latter case, the image contrast was absent entirely.

These observations confirm that our results, and particularly the image contrast in nano-vis, can be attributed to the optical absorption of the sample with a likely contribution from the thermal properties of the sample. Moreover, for a single domain of the sample, defects on HOPG or in MWCNTs increase the phonon scattering, which has an impact on the thermal conductivity of the sample and, therefore, also impacts the nano-vis contrast. This thermal contribution is discussed in

DOI: 10.1021/acsphotonics.8b00590
ACS Photonics XXXX, XXX, XXX−XXX

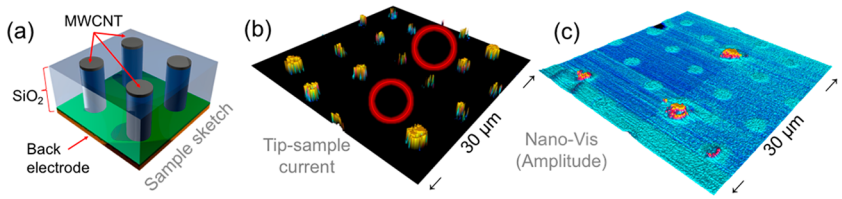

Figure 4. (a) Schematics of the MWCNT sample consisting of vertically grown nanotubes in a SiO_2 matrix. (b) CSAFM image showing a map of the tip−sample current obtained under 200 mV bias. The interconnects marked with circles show no current response. (c) Nano-vis image obtained simultaneously to the current showing a higher absorption than for the vias with no current.

more detail below. Regarding the role of the plasmonic tip, notice that the same kind of tip was experimentally shown to produce significant confinement of the electromagnetic field that allows obtaining optical spectroscopy images well beyond the diffraction limit of light.[6,29] We demonstrate the electric field localization and amplification by the sequential imaging with nano-vis and tip-enhanced Raman spectroscopy of a SiO_2/Si nanostructured sample. The results that are shown in Figure S8 evidence the nanoscale resolution of TERS and nano-vis; since the plasmonic effects of the tips used are critical for the nanoscale imaging capability of TERS, we expect that the same effects must also play a role in nano-vis. To definitively answer this question, a comparative nano-vis study using plasmonic and nonplasmonic tips could shed light on the role of plasmonic contributions to nano-vis. Moreover, the TERS results illustrate the possibility to combine nano-vis with other tip-enhanced methods and advanced scanning probe microscopy as shown below with electrical AFM.

Simultaneous Nano-vis and Electrical AFM: Defects in Carbon Nanotube Interconnects. After demonstrating the possibility to map the optical absorption and photothermal expansion with nanoscale resolution, as shown above, we aim now at exploiting this method to address a different question related to a technological challenge that concerns the development and application of multiwall carbon nanotube interconnects. This emerging technology has the potential to substitute conventional electronics based on copper through silicon vias. However, one issue of MWCNT interconnects is the contact resistance between the back-metal contact and the carbon nanotubes vertically grown in a SiO_2 matrix as shown in Figure 4a. In a previous work, we reported on the nanoscale characterization of such devices using conductive AFM (CSAFM), demonstrating the issue of contact resistance.[30]

CSAFM images of the current that flows through the AFM tip in response to a potential difference applied between the tip and the sample. However, the reason that some of the devices displayed poor electrical contact was not fully clear. To offer new insights into this question, an MWCNT interconnect sample was analyzed in real time with both nano-vis and CSAFM, providing the imaging results shown in Figure 4. The current map acquired during CSAFM shows the conductivity of MWCNT vias, although there are also two vias marked by circles in Figure 4b that do not conduct. In the nano-vis result in Figure 4c, we found a high contrast for some of the MWCNT vias. From the CSAFM and nano-vis results in Figure 4b and c we observe that the two vias that ultimately failed in conducting are precisely the same vias that show the highest nano-vis contrast. In fact, the electrical failure is related to the resistance issues for the circuit break with no indication of exactly where the break occurs, either between the MWCNT and the back electrode as previously reported or at the top side of the MWCNT with the tip. By comparing the current distribution with nano-vis, we must notice that the higher contrast in nano-vis observed for the vias that failed to conduct current should be a consequence of poor contact between the MWCNT and the back-metal electrode. In the absence of good contact with the back electrode, the MWCNT vias would be more thermally insulated in the SiO_2 matrix. Indeed, this observation opens one crucial question: how do the differences in heat dissipation affect the image contrast? This is a key point since understanding the role of heat dissipation opens perspectives toward using nano-vis for the quantification of thermal properties of materials at the nanoscale. For the sake of completeness, we must notice two vias situated on the left and bottom corners in Figure 4b,c, which show both good conductivity and nano-vis contrast. At the moment we cannot present a clear explanation for this, which demands further investigations. Answering these questions is currently the next step in our research. Meanwhile, in the last part of this work, we briefly discuss the heat dissipation contribution to the image contrast in nano-vis.

Defects and Heat Dissipation Contribution to Nano-vis. In Figure 2b, we see clearly resolved at the nanoscale that the MWCNT region is not homogeneous. The different structures that are blurred in the topography are discernible in the nano-vis image. To illustrate this point, we have marked a band region delimited by dashed lines in Figure S6a. While this band appears homogeneous with high topography, in the nano-vis image in Figure S6b we see other details not visible in topography. To understand these heterogeneities, we take a look at the MWCNT cross-section view by scanning electron microscopy of a similar structure previously reported by us and others; see Figure S6c.[30] We observe that the MWCNTs do not fill all the space in the vias but that there are some voids. One possible explanation for the heterogeneous contrast observed in nano-vis can be associated with the voids in the MWCNT region. Overall, there is some correlation between the height of the MWCNT and the nano-vis contrast; this is understandable since more material implies larger absorption and thus larger thermal expansion. However, the more detailed contrast that is not correlated to the topography can be related to subsurface features of the MWCNTs like the voids. This can be expected as due to two contributions from the voids to the image contrast. First, as discussed above, more material implies more chances the photons will be absorbed, resulting in larger thermal expansion. Second, the presence of voids below the surface induces a decrease in the thermal conductivity, which will then result in an increase in contrast due to a larger localized heat that cannot be so easily dissipated as in the regions without voids. Since these two contributions go in opposite directions in terms of thermal expansion, pinpointing the exact physical origin of this detailed contrast still eludes us. This indicates a line of study to be addressed in follow-up works. Under the hypothesis that the main contribution to

DOI: 10.1021/acsphotonics.8b00590
ACS Photonics XXXX, XXX, XXX−XXX

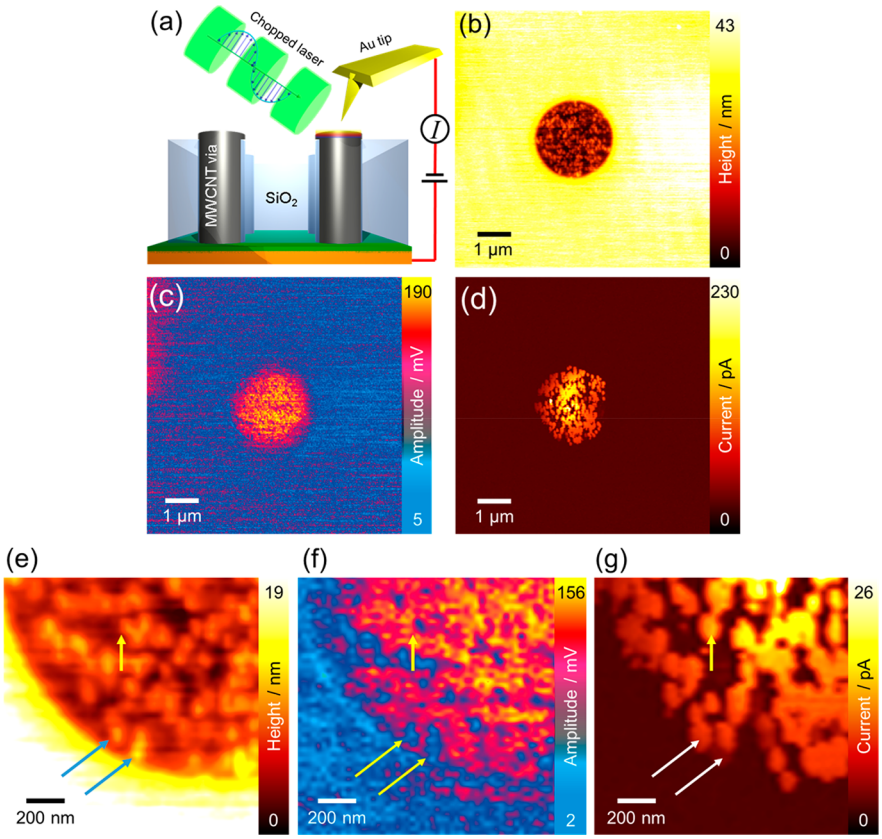

Figure 5. (a) Side-view sketch (nonscaled) of the MWCNT vias configuration during nano-vis and current sensing AFM. (b) Topography, (c) nano-vis, and current images of an MWCNT via interconnect and zoom-in images (e), (f), and (g) on the left bottom corner of the via in images (b)-(d).

heterogeneities observed is due to the differences in the amount of material, we then can attribute the different contrast in Figure 2 to the density of MWCNTs. Indeed, in the SEM cross-section image, we can see MWCNT bundles and voids.

If we consider the thermal conductivity of the MWCNT as a source of image contrast, then the defects should also play a role in nano-vis. The results of defects in carbon nanotubes would impact the thermal conductivity of the material, decreasing it. The reason behind this is the increase in phonon scattering with defects that decrease the thermal conductivity of graphene-like materials.[31]

Therefore, in addition to the increase in MWCNT density, we expect that defects further increase the contrast in nano-vis. This works the other way around too: if the MWCNT would have lower defects due to a gentler sample processing, for example, then the heat dissipation becomes larger, reducing the contrast in nano-vis. To investigate this further, we focus now on the MWCNT vias schematically shown in Figure 5a. The high-resolution imaging results of a single MWCNT via are displayed in Figure 5b−d for the topography, nano-vis, and CSAFM. In Figure 5e−g we present the zoom-in images for one part of the MWCNT via. It is worth noticing that the nano-vis images in Figure 5c,f do not correlate with the topography (Figure 5b,e) and only partially correlate with the current (Figure 5d,g); this observation excludes the presence of topographical artifacts. These images show clear distinctions between the MWCNT and the SiO_2 matrix, demonstrating once more the spatial resolution that can be obtained with nano-vis. We also observed structures that are resolved inside the MWCNT via, and it is particularly remarkable that we are able to see individual carbon nanotubes in all three images. Here again, we identify two different regimes for results shown in Figure 5. One, the main contribution to the photothermal expansion nano-vis images appears again to be dominated by the optical absorption of the sample. The optically transparent SiO_2 systematically shows a lower nano-vis contrast with respect to the carbon nanotubes. The second regime observed for changes in a single material is affected by the thermal properties of the sample. Depending on the processing of the MWCNT, we see that in one case with fewer defects on the MWCNT top surface we are able to resolve individual tubes (Figure 5). With fewer defects, the electrons and phonons have larger mobility, which is reflected in the current and nano-vis images, respectively; see Figure 5. We observe that the individual MWCNTs do not show the largest contrast in nano-vis results in Figure 5f. Notice that this was not the case for the AFM topography image for the sample shown in Figure 2, in which individual MWCNTs cannot be seen, but rather a nonhomogeneous and smooth surface. Another difference is the protrusion of the MWCNT region over the SiO_2, while for the via sample in Figure 4 the MWCNT topography is below the surface of the SiO_2 matrix. The current and nano-vis results in Figure 5 confirm the physical description illustrated in Figure 1a. That is, the electron−phonon scattering that follows optical absorption induces contrast due to the photothermal expansion of the sample transduced by the AFM cantilever. Differences in heat conductivity due to changes in a sample, such as increased defects or subsurface voids, also contribute to the contrast in nano-vis. The situation is different for the CSAFM results since the current observed in a via requires a certain degree of structural stability all along the MWCNT interconnect from the top down to the bottom electrode; see Figure S7.

DOI: 10.1021/acsphotonics.8b00590
ACS Photonics XXXX, XXX, XXX−XXX

PERSPECTIVES

Notice the reasons that we used the samples here reported as a model system for nano-vis: the MWCNT/SiO_2 have optically transparent and nontransparent domains[32,33] with minimal surface topography differences that minimize contributions from imaging artifacts. The major demonstration of being able to visualize at the nanoscale two materials with entirely different optical absorption is a necessary step toward applying nano-vis in the investigation of more complex systems at different wavelengths. A follow-up application and demonstration of our method includes the study of a mixture of semiconducting and metallic single-walled carbon nanotubes (SWCNTs) that have well-defined optical resonances at different wavelengths in the visible range. While the topography would show where the nanotubes are, by acquiring two sequential nano-vis images under red and green laser excitations, one could visualize the semiconducting and metallic SWCNTs. This is also interesting for the case of more complex systems such as hybrid two-dimensional materials since nano-vis could provide useful information on the coupling of plasmons in the visible range similarly to recent reports on two-dimensional heterostructures with PTIR.[19,34]

SUMMARY AND IMPLICATIONS

We demonstrated a novel, inexpensive, and general way to visualize the optical absorption and photothermal expansion using a conventional AFM. The spatial resolution of nano-vis imaging was obtained beyond the diffraction limit of light. This was demonstrated in the two-sample systems studied in this work: a semiconducting 2D material and metallic MWCNTs. The remarkable resolution with values as good as ~4 nm was found to be at least as good or even better than the topographic image in AFM but providing complementary information about the sample. This development opens the door for the low-cost analysis and characterization of optical and electronic properties of nontransparent samples at the nanoscale. It is worth noticing that the visualization of optical absorption at the nanoscale remained a challenging task that our work now simplifies.

The method here reported contributes to the development of novel ways for nanoscale characterization by paving the way to the inexpensive and widespread integration of nano-vis in conventional AFM devices. This opens now new possibilities for AFM as a toolbox with optics making a tremendous impact in key fields from cell biology[35] to energy harvesting,[36] for example, by making the visualization of nonradiative recombination in organic solar cells possible[37] and the study of thermoelectric materials,[38] providing simultaneous nanoscale information on the thermal and electrical conductivities.

MATERIALS AND METHODS

A conventional AFM (5420) from Keysight Technologies was coupled with a semiconductor cw laser modulated by a tunable mechanical chopper with a maximum chopping rate of 10 kHz. The laser beam of 514.7 nm (2.41 eV) with an intensity of 6 mW was focused on the tip−sample region using a 10× LWD objective (NA 0.2). The fine focus is controlled using a piezoelectric steering mirror and a piezoelectric linear motor to adjust the spot focus at the tip/sample region. For the MWCNT interconnects and the CSAFM results an AIST-NT Omega Scope AFM was used, with a side illumination laser excitation at 532 nm wavelength focused on the tip with a 100× LWD objective (NA 0.7).

The Cantilever. The resonance frequency f_0 of a rectangular cross-sectioned cantilever depends on its geometry (length l and thickness h), density ρ, and its Young's modulus E according to the expression[39] $f_0 \propto \sqrt{\frac{E}{\rho}}\frac{h}{l^2}$. Therefore, our first concern regarding the possibility to obtain a Au cantilever with the proper resonance frequency implied tuning the cantilever dimensions, in particular by increasing its length due to the inverse square root dependence on this parameter.

Finite element method simulation results in Figure S1a of the Supporting Information showed that a length on the order of 1000 μm should provide oscillation frequencies compatible with those of the mechanical chopper. This was experimentally verified as shown in Figure S1b by measuring the resonance spectrum of such long cantilevers using the built-in piezoelectric excitation by the AFM. Following a previously reported method,[24] we reproducibly obtained cantilevers with resonance frequencies below 10 kHz (see Figure S1b). Scanning electron microscopy images of the cantilever and the tip apex are shown in Figure 6. The second challenge was using these cantilevers in our nano-vis setup in a side-illumination configuration. The configuration of the tip−sample and laser is shown in the sketch in Figure 1b.

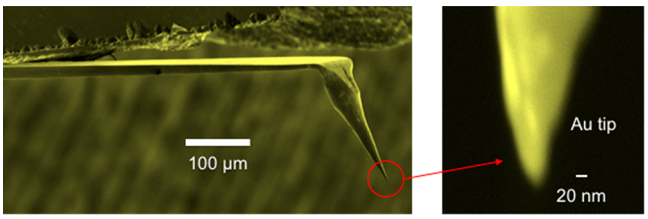

Figure 6. Scanning electron microscopy imaging of the fully metallic cantilever and zoom-in on the tip apex.

The Samples. The MWCNT sample in SiO_2 is an excellent sample for testing purposes given the clear separation between the two materials and the contrast between optical absorption and thermal coefficients of MWCNTs and SiO_2. The SiO_2 has very low absorption under the laser excitation used and therefore is expected to induce a much lower deflection amplitude of the cantilever. For the MWCNT region, the contrast is expected to be much higher as a direct consequence of higher absorption.

To prove the applicability of this method, we tested our system with another sample, GaSe on HOPG. We chose GaSe not only because of its well-defined interface with HOPG but also because it has an energy band gap of about 2 eV (see Figure S2 in the Supporting Information), so the green excitation at 2.41 eV is above the absorption edge, ensuring that a significant number of photons get absorbed. The other important reason for using GaSe as a relevant system is that its surface is atomically flat. The consequence of this flatness is that it minimizes any contribution to the cantilever oscillation (nano-vis) originating from changes in topography (cross-talk and other imaging artifacts).

ASSOCIATED CONTENT

Supporting Information

The Supporting Information is available free of charge on the ACS Publications website at DOI: 10.1021/acsphotonics.8b00590.

DOI: 10.1021/acsphotonics.8b00590
ACS Photonics XXXX, XXX, XXX−XXX

Numerical simulations of the cantilever oscillation, the optical absorption of GaSe, and effects of chopping frequency and illumination (PDF)

■ AUTHOR INFORMATION

Corresponding Author

*E-mail (R. D. Rodriguez): raulmet@gmail.com.

ORCID

Raul D. Rodriguez: 0000-0003-4016-1469

Evgeniya Sheremet: 0000-0003-3937-8628

Author Contributions

R.D.R. conceived, designed, and implemented the experiments and wrote the manuscript draft. T.I.M. and E.B. contributed to the realization of experiments and analysis of the results. E.S. contributed to the design and conception of this work. H.S. and Y.P. contributed to the experimental implementation of nano-vis. A.M. contributed to the realization of the nano-vis and CSAFM experiments on the MWCNT vias. R.D.R., M.H., and D.R.T.Z. assisted with the supervision of this work, proof-reading the manuscript, and the interpretation of the experimental results. All authors read and approved the manuscript.

Notes

The authors declare no competing financial interest.

■ ACKNOWLEDGMENTS

We are grateful to Yuva Prasad and Harsha Shah for critical help in the acquisition of the experimental data. We thank Suhail Shah for proofreading the manuscript; Adan Lopez for the optical absorption data of GaSe and the bulk crystal; Holger Fielder, Sascha Hermann, and Stefan Schulz for the MWCNT sample; and Lukas Eng for fruitful discussions. We acknowledge funding by the German Science Foundation DFG Research Unit SMINT FOR1317 and by the Cluster of Excellence "Center for Advancing Electronics Dresden" (cfaed) and the COST action MP1302 on NanoSpectroscopy supported by COST (European Cooperation in Science and Technology). E.S. and R.D.R. thank the Tomsk Polytechnic University Competitiveness Enhancement Program grant.

■ REFERENCES

(1) Hell, S. W.; Wichmann, J. Breaking the diffraction resolution limit by stimulated emission: stimulated-emission-depletion fluorescence microscopy. *Opt. Lett.* **1994**, *19* (11), 780−782.

(2) Betzig, E.; Trautman, J.; Weiner, J.; Harris, T.; Wolfe, R. Polarization contrast in near-field scanning optical microscopy. *Appl. Opt.* **1992**, *31* (22), 4563−4568.

(3) Heinzelmann, H.; Pohl, D. W. Scanning near-field optical microscopy. *Appl. Phys. A: Solids Surf.* **1994**, *59* (2), 89−101.

(4) Betzig, E. Single Molecules, Cells, and Super-Resolution Optics (Nobel Lecture). *Angew. Chem., Int. Ed.* **2015**, *54* (28), 8034−8053.

(5) Nowak, D.; Morrison, W.; Wickramasinghe, H. K.; Jahng, J.; Potma, E.; Wan, L.; Ruiz, R.; Albrecht, T. R.; Schmidt, K.; Frommer, J.; Sanders, D. P.; Park, S. Nanoscale chemical imaging by photoinduced force microscopy. *Science Advances* **2016**, *2* (3), e1501571.

(6) Sheremet, E.; Rodriguez, R. D.; Agapov, A. L.; Sokolov, A. P.; Hietschold, M.; Zahn, D. R. T. Nanoscale imaging and identification of a four-component carbon sample. *Carbon* **2016**, *96*, 588−593.

(7) Rahaman, M.; Rodriguez, R. D.; Plechinger, G.; Moras, S.; Schuller, C.; Korn, T.; Zahn, D. R. T. Highly Localized Strain in a MoS2/Au Heterostructure Revealed by Tip-Enhanced Raman Spectroscopy. *Nano Lett.* **2017**, *17* (10), 6027−6033.

(8) Olson, J.; Dominguez-Medina, S.; Hoggard, A.; Wang, L.-Y.; Chang, W.-S.; Link, S. Optical characterization of single plasmonic nanoparticles. *Chem. Soc. Rev.* **2015**, *44* (1), 40−57.

(9) Durig, U.; Pohl, D. W.; Rohner, F. NEAR-FIELD OPTICAL-SCANNING MICROSCOPY. *J. Appl. Phys.* **1986**, *59* (10), 3318−3327.

(10) Langelüddecke, L.; Singh, P.; Deckert, V. Exploring the nanoscale: fifteen years of tip-enhanced Raman spectroscopy. *Appl. Spectrosc.* **2015**, *69* (12), 1357−1371.

(11) Katzenmeyer, A. M.; Holland, G.; Kjoller, K.; Centrone, A. Absorption Spectroscopy and Imaging from the Visible through Mid-Infrared with 20 nm Resolution. *Anal. Chem.* **2015**, *87* (6), 3154−3159.

(12) Pohl, D. W.; Denk, W.; Lanz, M. Optical stethoscopy: Image recording with resolution $\lambda/20$. *Appl. Phys. Lett.* **1984**, *44* (7), 651−653.

(13) Zenhausern, F.; O'boyle, M.; Wickramasinghe, H. Apertureless near-field optical microscope. *Appl. Phys. Lett.* **1994**, *65* (13), 1623−1625.

(14) Fischer, U. C.; Pohl, D. Observation of single-particle plasmons by near-field optical microscopy. *Phys. Rev. Lett.* **1989**, *62* (4), 458.

(15) Lahiri, B.; Holland, G.; Aksyuk, V.; Centrone, A. Nanoscale Imaging of Plasmonic Hot Spots and Dark Modes with the Photothermal-Induced Resonance Technique. *Nano Lett.* **2013**, *13* (7), 3218−3224.

(16) Dazzi, A.; Prater, C. B.; Hu, Q.; Chase, D. B.; Rabolt, J. F.; Marcott, C. AFM−IR: combining atomic force microscopy and infrared spectroscopy for nanoscale chemical characterization. *Appl. Spectrosc.* **2012**, *66* (12), 1365−1384.

(17) Chae, J.; Dong, Q.; Huang, J.; Centrone, A. Chloride Incorporation Process in CH3NH3PbI3−xClx Perovskites via Nano-scale Bandgap Maps. *Nano Lett.* **2015**, *15* (12), 8114−8121.

(18) Lu, F.; Jin, M. Z.; Belkin, M. A. Tip-enhanced infrared nanospectroscopy via molecular expansion force detection. *Nat. Photonics* **2014**, *8* (4), 307−312.

(19) Barcelos, I. D.; Cadore, A. R.; Alencar, A. B.; Maia, F. C. B.; Mania, E.; Oliveira, R. F.; Bufon, C. C. B.; Malachias, Â.; Freitas, R. O.; Moreira, R. L.; Chacham, H. Infrared Fingerprints of Natural 2D Talc and Plasmon−Phonon Coupling in Graphene−Talc Heterostructures. *ACS Photonics* **2018**, *5*, 1912.

(20) Dazzi, A.; Prater, C. B. AFM-IR: technology and applications in nanoscale infrared spectroscopy and chemical imaging. *Chem. Rev.* **2017**, *117* (7), 5146−5173.

(21) Rice, J. H. Nanoscale optical imaging by atomic force infrared microscopy. *Nanoscale* **2010**, *2* (5), 660−667.

(22) Rodriguez, R. D.; Müller, S.; Sheremet, E.; Zahn, D. R. T.; Villabona, A.; Lopez-Rivera, S. A.; Tonndorf, P.; de Vasconcellos, S. M.; Bratschitsch, R. Selective Raman modes and strong photo-luminescence of gallium selenide flakes on sp2 carbon. *J. Vac. Sci. Technol., B: Nanotechnol. Microelectron.: Mater., Process., Meas., Phenom.* **2014**, *32* (4), 04E106.

(23) Fiedler, H.; Toader, M.; Hermann, S.; Rodriguez, R. D.; Sheremet, E.; Rennau, M.; Schulze, S.; Waechtler, T.; Hietschold, M.; Zahn, D. R. T. Carbon nanotube based via interconnects: Performance estimation based on the resistance of individual carbon nanotubes. *Microelectron. Eng.* **2014**, *120*, 210−215.

(24) Rodriguez, R. D.; Sheremet, E.; Muller, S.; Gordan, O. D.; Villabona, A.; Schulze, S.; Hietschold, M.; Zahn, D. R. T. Compact metal probes: a solution for atomic force microscopy based tip-enhanced Raman spectroscopy. *Rev. Sci. Instrum.* **2012**, *83* (12), 123708.

(25) Kolchuzhin, V.; Mehner, J.; Sheremet, E.; Kunal, B.; Rodriguez, R. D.; Zahn, D. R. T. In *Understanding tip-enhanced Raman spectroscopy by multiphysics finite element simulations*, 2015 16th International Conference on Thermal, Mechanical and Multi-Physics Simulation and Experiments in Microelectronics and Microsystems (EuroSimE); IEEE, 2015; pp 1−5.

DOI: 10.1021/acsphotonics.8b00590
ACS Photonics XXXX, XXX, XXX−XXX

(26) Reddick, R.; Warmack, R.; Ferrell, T. New form of scanning optical microscopy. *Phys. Rev. B: Condens. Matter Mater. Phys.* **1989**, *39* (1), 767.
(27) Greco, S.; Dal Zilio, S.; Bek, A.; Lazzarino, M.; Naumenko, D. Frequency Modulated Raman Spectroscopy. *ACS Photonics* **2018**, *5*, 312.
(28) Zhu, H.; Yi, F.; Cubukcu, E. Plasmonic metamaterial absorber for broadband manipulation of mechanical resonances. *Nat. Photonics* **2016**, *10* (11), 709−714.
(29) Kolchuzhin, V. A.; Sheremet, E.; Bhattacharya, K.; Rodriguez, R. D.; Paul, S. D.; Mehner, J.; Hietschold, M.; Zahn, D. R. T. Mechanical properties and applications of custom-built gold AFM cantilevers. *Mechatronics* **2016**, *40*, 281−286.
(30) Fiedler, H.; Toader, M.; Hermann, S.; Rodriguez, R. D.; Sheremet, E.; Rennau, M.; Schulze, S.; Waechtler, T.; Hietschold, M.; Zahn, D. R. T. Distinguishing between individual contributions to the via resistance in carbon nanotubes based interconnects. *ECS J. Solid State Sci. Technol.* **2012**, *1* (6), M47−M51.
(31) Hao, F.; Fang, D.; Xu, Z. Mechanical and thermal transport properties of graphene with defects. *Appl. Phys. Lett.* **2011**, *99* (4), 041901.
(32) Rodríguez-de Marcos, L. V.; Larruquert, J. I.; Méndez, J. A.; Aznárez, J. A. Self-consistent optical constants of SiO2 and Ta2O5 films. *Opt. Mater. Express* **2016**, *6* (11), 3622−3637.
(33) Yu, J.; Grossiord, N.; Koning, C. E.; Loos, J. Controlling the dispersion of multi-wall carbon nanotubes in aqueous surfactant solution. *Carbon* **2007**, *45* (3), 618−623.
(34) Brown, L. V.; Davanco, M.; Sun, Z.; Kretinin, A.; Chen, Y.; Matson, J. R.; Vurgaftman, I.; Sharac, N.; Giles, A. J.; Fogler, M. M.; Taniguchi, T.; Watanabe, K.; Novoselov, K. S.; Maier, S. A.; Centrone, A.; Caldwell, J. D. Nanoscale Mapping and Spectroscopy of Nonradiative Hyperbolic Modes in Hexagonal Boron Nitride Nanostructures. *Nano Lett.* **2018**, *18* (3), 1628−1636.
(35) Shan, Y.; Wang, H. The structure and function of cell membranes examined by atomic force microscopy and single-molecule force spectroscopy. *Chem. Soc. Rev.* **2015**, *44* (11), 3617−3638.
(36) Tennyson, E. M.; Gong, C.; Leite, M. S. Imaging Energy Harvesting and Storage Systems at the Nanoscale. *ACS Energy Letters* **2017**, *2* (12), 2761−2777.
(37) Benduhn, J.; Tvingstedt, K.; Piersimoni, F.; Ullbrich, S.; Fan, Y.; Tropiano, M.; McGarry, K. A.; Zeika, O.; Riede, M. K.; Douglas, C. J. Intrinsic non-radiative voltage losses in fullerene-based organic solar cells. *Nature Energy* **2017**, *2* (6), 17053.
(38) Zhu, T.; Liu, Y.; Fu, C.; Heremans, J. P.; Snyder, J. G.; Zhao, X. Compromise and Synergy in High-Efficiency Thermoelectric Materials. *Adv. Mater.* **2017**, *29* (14), 1605884.
(39) Butt, H. J.; Cappella, B.; Kappl, M. Force measurements with the atomic force microscope: Technique, interpretation and applications. *Surf. Sci. Rep.* **2005**, *59* (1−6), 1−152.

DOI: 10.1021/acsphotonics.8b00590
ACS Photonics XXXX, XXX, XXX−XXX